Statistical estimation with Kronecker products in positron emission tomography

John A.D. Aston [a], Roger N. Gunn [b,*,1]

[a]*Statistical Research Division, US Bureau of the Census, Washington, DC 20233, USA*
[b]*Montreal Neurological Institute, McConnell Brain Imaging Center, McGill Univerisity, 3801 University St., Montreal, Que., Canada H3A 2B4*

Abstract

A method for linear statistical analysis of multidimensional imaging data is presented. It is applicable for a class of design and covariance matrices which involve Kronecker products. An efficient algorithm which allows for application of the method to large multidimensional data volumes is given. This has direct application to neuroimaging, and here the technique is applied to positron emission tomography (PET) data. PET is an in vivo functional imaging technique that measures biological processes such as blood flow and receptor concentrations. Here, the algorithm is used to correct for resolution degradation in these images. This process is typically referred to as PET partial volume correction. Examples involving both measured phantom and human data are given. This rapid algorithm leads to advances in the types of quantitative brain imaging studies that can be performed.
© 2003 Elsevier Inc. All rights reserved.

Keywords: Kronecker product; Linear models; Positron emission tomography; Partial volume correction

1. Introduction

Estimation through the use of linear models is a fundamental technique in statistics. A linear model can be used to form the simplest regression through to the most

complex analysis of variance, by specification of appropriate design and covariance matrices. However, in the case of large data sets with complex inner structures, the design and covariance matrices are often difficult to handle computationally.

This paper investigates methods for a specific class of matrices which can be formed from Kronecker products of other smaller matrices. Taking advantage of these properties allows for the efficient application of linear models to multidimensional data sets, which would otherwise involve large matrices (e.g. 10^6 in each dimension).

Matrices of this class are routinely used in functional neuroimaging. Positron emission tomography (PET) is one such technique (see Fig. 1) which enables researchers to study the function of the human brain in vivo [1,2]. After intravenous injection of a radiolabelled compound of interest, it is possible to record the subsequent spatial and temporal radioactivity distribution using a ring of external gamma detectors [3]. This is based on recording the projection data (coincident gamma rays) and subsequently reconstructing three-dimensional image volumes for each temporal time frame to generate a four-dimensional dynamic data set (see Leahy and Qi [4] for a description of the PET reconstruction process). The application of bio-mathematical models to these 4-D data sets enables the estimation of 3-D images of the biological parameters [5]. Common applications include the measurement of blood flow, glucose metabolism and receptor concentrations. However, the resolution of these images is limited by the intrinsic properties of the scanner. Linear methods can be used to recover the data at a local level, using a characterisation of the point spread function, and adjunct structural data. To put the technique in context, a 3-D PET image volume typically contains about $128 \times 128 \times 64$ voxels (a voxel is a 3-D generalisation of a pixel whose size is about $2 \times 2 \times 4$ mm^3). The blurring of the data introduced by the tomograph is of the order of 6 mm full width half maximum (FWHM) in each direction.

The methods presented here allow for the application of resolution recovery techniques to PET data on a local level which improve the quantitative nature of the final results and allow further interpretation of the data than was previously possible. In PET, this technique is known as partial volume correction [6] and assumes a homogeneous radioactivity concentration in a set of regions defined from an anatomical parcellation of the brain using structural magnetic resonance imaging (MRI) data.
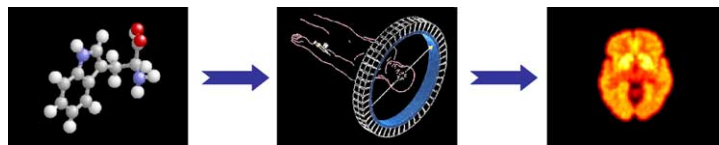

Fig. 1. Positron emission tomography (PET)—A radiolabelled compound of interest is injected intravenously in a subject of interest. The compounds spatial distribution is measured within a PET tomograph (a ring of gamma detectors wired up to detect coincident events). This generates three-dimensional image volumes of the radiotracers concentration.

This parcellation can be extended, by applying tissue classification techniques to the MRI data, to account for tissue type (such as grey and white matter) as well as the gross anatomical structures (such as cerebellum, striatum etc). The resultant technique will allow assessment of biological parameters even in cases where the brain structure is complex due to disease or abnormality, areas which are often the focus of neurological research i.e. it will allow for an assessment of true functional changes by removing the effect of confounding structural changes.

2. Theory

The method is primarily developed from the structural limitations imposed by the PET data. The tomographic scanner can be modelled as a three-dimensional linear filter, which spreads a point (in the object) over an area (in the reconstructed image). For these scanners, it is possible to describe this filter by a separate function in each of the three dimensions. The function that describes the blurring operator can be constructed as a convolution of the blurring kernels in each dimension, i.e. the point spread function is separable. This does not imply that the blurring model is spatially invariant, but merely that each direction can be modelled separately.

The design matrix requires information about the local anatomical neighbourhood. Higher resolution structural MRI data allows for the accurate determination of these anatomical regions based on their location and tissue type [7]. These images are coregistered to the PET images using a mutual information technique [8]. The regions are assumed to be homogeneous, that is, within each region there is a constant level of radiotracer, subject to noise. For a one-dimensional signal the problem can be formulated as

$$PRx + \varepsilon = b, \quad \varepsilon \sim N(0, \Sigma), \tag{1}$$

where P is a non-singular matrix characterising the filter (or point spread function), R is a matrix of full column rank containing the region definitions, x contains the true mean regional concentrations, ε is the noise in the data, and b is the PET data. Σ is the covariance matrix of the noise in the data, and is assumed to be positive definite.

Fig. 2 gives a graphical representation of this PET resolution recovery problem for a slice of the three-dimensional image volume. The goal is to estimate x, the true radiotracer concentration within each structurally defined region, from the PET data.

This could, in theory, be solved by vectorisation of the image volume which transforms the problem into the form of Eq. (1). Whilst this is not practically possible for PET image volumes, it can be helpful to discuss the problem in this way before moving onto the multimatrix operator approach which provides a viable solution.

2.1. One-dimensional implementation

For a one-dimensional implementation, images are vectorised, and the inherent three-dimensional structure of the image volume is ignored. The problem is simply
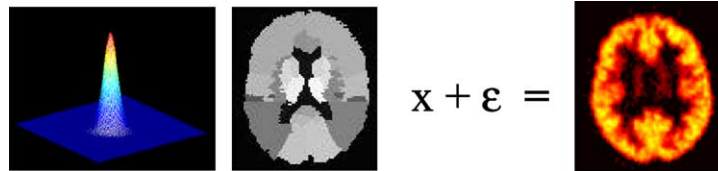
Fig. 2. Partial volume correction scheme. Images are (left to right) Filter (or Point Spread Function); Anatomical Region Definitions; Reconstructed PET Image. x represents the true regional radiotracer concentrations and ε the noise. Whilst this figure represents the general scheme, in practice the region definitions are more complex and in addition account for different tissue types.

described by Eq. (1). If the image size is a $k \times m \times n$, then b is a $kmn \times 1$ vector, but more importantly P and Σ are $kmn \times kmn$ matrices. R has dimension $kmn \times r$ and x dimension $r \times 1$ where r is the number of regions identified, and $r \ll kmn$.

Using weighted least squares allows x to be estimated as

$$\hat{x} = \left(R^{\mathrm{T}} P^{\mathrm{T}} \Sigma^{-1} P R \right)^{-1} R^{\mathrm{T}} P^{\mathrm{T}} \Sigma^{-1} b. \tag{2}$$

However, whilst this is theoretically straightforward, in practice its computation is compromised by the size of the matrices.

2.2. Multimatrix operator implementation

Here, multimatrix operations are defined. These are the operations of a set of matrices on a volume in order to replicate the operation of a much larger single matrix on a vectorisation of the volume. Convolutions or Kronecker products are well known to be applicable to image volumes. For instance, this is true in the field of wavelets where wavelet filters are operated dimension by dimension.

The use of multimatrix operators is required to provide an efficient calculation of products of the form

$$(P_1 \otimes P_2 \otimes \cdots \otimes P_n)q, \tag{3}$$

where the P_i are matrices and q is a vector. In the case where $n = 2$,

$$(P_1 \otimes P_2)q = \mathrm{vec}(P_2 \, \mathrm{unvec}(q) \, P_1^{\mathrm{T}}), \tag{4}$$

where $\mathrm{vec}(X)$ stacks the columns of a matrix X and unvec is an appropriate inverse operation of vec [9, Section 4.5.5]. This result generalizes for larger values of n.

Such multimatrix operators can be applied to a three-dimensional image volume ($n = 3$). A three-dimensional point spread operator is constructed as the operation of one small matrix in each of the three dimensions (cf. r.h.s of Eq. (4))

$$P = P_x \otimes P_y \otimes P_z, \tag{5}$$

where P_x, P_y, P_z are separable point spread matrices in the x, y, and z, directions respectively (see Fig. 3).
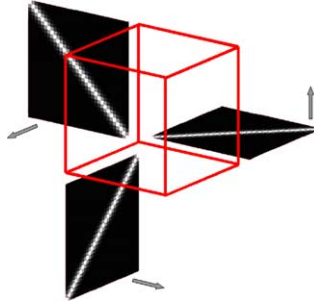
Fig. 3. Multimatrix point spread operator (P). The three-dimensional box represents the image volume (b), and the arrows indicate the direction of operation of the constituent matrices (P_x, P_y, P_z) on the multidimensional volume. The constituent matrices operate on each slice taken in the same orientation as the matrix before moving to the next slice.

2.3. Covariance structures

The use of the multimatrix operator is of importance, not only, in the operation on the image volume and regional definition, but also, as a component of the covariance matrix. The class of covariance matrices that are of interest here (characterisation of noise in a PET image) consist of two additive components. The first noise component is a spatially uncorrelated component (D_1, a diagonal matrix). The second is a spatially correlated component which results from the intrinsic noise in the data source and follows a Poisson distribution. However, as there are a large number of counts, they can be treated as a signal dependent normally distributed noise component ($P D_2 P^{\mathrm{T}}$ where D_2 is also diagonal).

Eq. (1) can be rearranged to give

$$Rx + \eta = P^{-1}b, \quad \eta \sim N(0, P^{-1}\Sigma(P^{-1})^{\mathrm{T}}). \tag{6}$$

This is a theoretical construct, as opposed to a practical implementation, because a deconvolution of the filter is unstable due to the first noise (uncorrelated) component in the data. However, this representation will lead to an algorithm where the squared blurring operator (P^2) is involved as opposed to the squared deconvolution operator (P^{-2}) which is inherently less stable. In this framework, $\Sigma_2 = P^{-1}\Sigma(P^{-1})^{\mathrm{T}}$ is defined to be of the following form:

$$\Sigma_2 = P^{-1}(D_1 + P D_2 P^{\mathrm{T}})(P^{-1})^{\mathrm{T}} = P^{-1}D_1(P^{-1})^{\mathrm{T}} + D_2, \tag{7}$$

where D_2 is the signal dependent variance component (which can be approximated by Rx). The structure for Σ_2 is derived from the properties of the two noise components, the intrinsic (D_2) and the reconstruction and measurement ($P^{-1}D_1(P^{-1})^{\mathrm{T}}$). D_1 and D_2 are positive definite diagonal matrices. Thus our estimate for the true concentrations becomes

$$\hat{x} = \left(R^{\mathrm{T}}(P^{-1}D_1(P^{-1})^{\mathrm{T}} + D_2)^{-1}R\right)^{-1} \\ \times R^{\mathrm{T}}(P^{-1}D_1(P^{-1})^{\mathrm{T}} + D_2)^{-1}P^{-1}b. \tag{8}$$

A similar expression can be derived for the variance of the estimates. If $W = \Sigma_2^{-1}$ then

$$\text{var}(\hat{x}) = \frac{\left(R^{\mathrm{T}}WR\right)^{-1}(R\hat{x} - P^{-1}b)^{\mathrm{T}}W(R\hat{x} - P^{-1}b)}{kmn - r}. \tag{9}$$

However, there is a problem with the calculation of these estimates. While the matrices which combine to make P can easily be defined in the multimatrix form above, Σ_2 contains a sum of two different components. The individual components are easy to operate but the inverse of their combination is not. However, the following solution is proposed. If

$$Z = WR = (P^{-1}D_1(P^{-1})^{\mathrm{T}} + D_2)^{-1}R, \tag{10}$$

then

$$W^{-1}Z = P^{-1}D_1(P^{-1})^{\mathrm{T}}Z + D_2Z = R, \tag{11}$$

Eq. (11) can be solved iteratively for Z using the multimatrix structure of P and diagonal properties of D_1 and D_2.

2.3.1. Iterative method

A first-order stationary iterative scheme was chosen

$$Z_{n+1} = Z_n - \tau C^{-1}(W^{-1}Z_n - R), \tag{12}$$

where C is a non-singular matrix and τ is the relaxation parameter which will ensure convergence given C and W (see below). If C is chosen to be $P^{-1}D_1(P^{-1})^{\mathrm{T}}$ then the algorithm is

$$Z_{n+1} = (1 - \tau)Z_n + \tau P^{\mathrm{T}}D_1^{-1}P(R - D_2Z_n). \tag{13}$$

The solution Z is then incorporated into the weighted least squares solution as

$$\hat{x} = (Z^{\mathrm{T}}R)^{-1}Z^{\mathrm{T}}P^{-1}b, \tag{14}$$

and for the variance estimate as

$$\text{var}(\hat{x}) = \frac{(Z^{\mathrm{T}}R)^{-1}Z^*(R\hat{x} - P^{-1}b)}{kmn - r}, \tag{15}$$

where $Z^* = (R\hat{x} - P^{-1}b)^{\mathrm{T}}W$ is solved using the same iterative procedure as the one above with R replaced by $(R\hat{x} - P^{-1}b)$.

2.3.2. Convergence

Let $C = P^{-1}D_1(P^{-1})^{\mathrm{T}}$ and $W = (P^{-1}D_1(P^{-1})^{\mathrm{T}} + D_2)^{-1}$ as above. Then the iterative scheme (Eq. (13)) is given by

$$Z_{n+1} = Z_n + \tau C^{-1}(R - W^{-1}Z_n). \tag{16}$$

If C^{-1} and W^{-1} are positive definite (which is elementary from their definitions) then the iterative scheme will converge for $0 < \tau < \frac{2}{\lambda_{\max}(C^{-1}W^{-1})}$ where $\lambda_{\max}(\cdot)$ is the maximal eigenvalue [10, Theorem 5.6]. Thus, to guarantee convergence, it

remains to calculate an upper bound for the maximal eigenvalue of $C^{-1}W^{-1}$ which enables an appropriate selection of τ.

$$
\begin{aligned}
C^{-1}W^{-1} &= P^{\mathrm{T}}D_1^{-1}P(D_2 + P^{-1}D_1(P^{-1})^{\mathrm{T}}) \\
&= P^{\mathrm{T}}D_1^{-1}PD_2 + I.
\end{aligned}
\tag{17}
$$

A corollary [10, Corollary 3.14] of the Courant–Fischer theorem [10, Lemma 3.13] gives an upper bound for the maximal eigenvalue in the case of a product of a positive definite matrix (D_1^{-1} or D_2) and a matrix with non-negative maximal eigenvalue (P). The addition of the identity matrix I simply adds 1 to the bound, giving

$$
\lambda_{\max}(C^{-1}W^{-1}) \leqslant \lambda_{\max}(D_1^{-1})\ \lambda_{\max}(P^{\mathrm{T}}P)\ \lambda_{\max}(D_2) + 1,
\tag{18}
$$

where $\lambda_{\max}(D_i)$ is the largest element of the diagonal matrix D_i and $\lambda_{\max}(P^{\mathrm{T}}P)$ is the square of the maximum singular value of P. Thus $s_{\max}(P) = \sqrt{\lambda_{\max}(P^{\mathrm{T}}P)}$, which is just the product of the maximal singular values of each individual matrix component of P. The singular values of the Kronecker product are the product of the singular values of the individual component matrices [11]. For example for a Kronecker product matrix P

$$
\begin{aligned}
P = P_1 \otimes P_2 &= (U_1 S_1 V_1{}^{\mathrm{T}}) \otimes (U_2 S_2 V_2{}^{\mathrm{T}}) \\
&= (U_1 \otimes U_2)(S_1 \otimes S_2)(V_1^{\mathrm{T}} \otimes V_2^{\mathrm{T}}) = USV^{\mathrm{T}}.
\end{aligned}
\tag{19}
$$

An alternative derivation of Eq. (18) arises from the matrix norm

$$
\begin{aligned}
\lambda_{\max}(C^{-1}W^{-1}) &\leqslant ||C^{-1}W^{-1}||_2 \leqslant ||P^{\mathrm{T}}||_2\ ||D_1^{-1}||_2\ ||P||_2\ ||D_2||_2 + ||I||_2 \\
&= \lambda_{\max}(D_1^{-1})\ \lambda_{\max}(P^{\mathrm{T}}P)\ \lambda_{\max}(D_2) + 1
\end{aligned}
\tag{20}
$$

A value for τ that guarantees convergence of the iterative scheme, although not necessarily optimal, can then be chosen as

$$
\tau = \frac{2}{\lambda_{\max}(D_1^{-1})\ s_{\max}(P)^2\ \lambda_{\max}(D_2) + 2}.
\tag{21}
$$

2.3.3. Special case

If there is no signal dependent component ($D_2 = 0$), the weighting matrix reduces down to

$$
W = (P^{-1}D_1(P^{-1})^{\mathrm{T}})^{-1} = P^{\mathrm{T}}D_1^{-1}P.
\tag{22}
$$

In this special case, the solution is explicit and does not require an iterative approach. The solution then becomes

$$
\hat{x} = \left(R^{\mathrm{T}}P^{\mathrm{T}}D_1^{-1}PR\right)^{-1} R^{\mathrm{T}}P^{\mathrm{T}}D_1^{-1}b,
\tag{23}
$$

which can be determined solely using the multimatrix methods above. The special case can be used to construct an initialization (Z_0) for the iterative method with

more complex noise models. The iterative process can be initialized with $Z_0 = P^T D_1^{-1} P R$ which is calculated using the multimatrix method. Similarly, for the variance estimation, $Z_0^* = (R\hat{x} - P^{-1}b)^T P^T D_1^{-1} P$ can be used for the initialization.

This special case can occur when partial volume correction is being applied to a parametric image generated from previous kinetic modelling of the data (here b is a parametric image). Kinetic modelling can include weighting factors that account for signal dependent noise in the data. With linear kinetic models the two phases of analysis (temporal modeling and partial volume correction) can be interchanged without effecting the parameter estimates. When non-linear models are used and the temporal modelling is applied before partial volume correction the resulting parameters are a good approximation as opposed to being exact (see Gunn et al. [5] for a description of PET kinetic modelling).

3. Examples

The partial volume problem is an important problem for quantitative PET imaging which arises from the limited resolution of the scanner. In essence, regions of differing concentrations get blurred together making it difficult to accurately estimate the true concentration in each region. However, the process is also noisy and it is not possible to remove the blurring through a simple deconvolution of the blurring operator due to ill-conditioning.

Measured phantom and human PET data have been acquired for validation and subsequent application of the methods developed here [12]. The iterative approach, with a complex noise model, is applied to a phantom data set and the direct multimatrix method, with a simple noise model, is applied to human brain data.

3.1. Phantom data

Cylindrical syringes were scanned to verify the effectiveness of the recovery in known situations of partial volume (i.e. a simple geometry involving a homogeneous radioactivity concentration which is known). Four different syringes were scanned each with a different inner diameter (15, 12, 9, 5 mm), each containing a solution of known radioactive concentration. The blurring kernel of the scanner is 6 mm in the $x-y$ directions and 6.5 mm in the z-direction. The P matrices are characterised from empirical measurements performed on the scanner with a point source, D_2 is proportional to the measured counts and D_1 was assumed to be a multiple of the identity matrix, where the multiplier is determined from the background of the image. τ was calculated using Eq. (21) as 0.0911 ($s_{\max}(P_x) = 0.9994$, $s_{\max}(P_y) = 0.9994$, $s_{\max}(P_z) = 1$, $s_{\max}(P) = 0.9989$, $\lambda_{\max}(D_1^{-1}) = 0.0007321$, $\lambda_{\max}(D_2) = 27320$). This is not necessarily an optimal value but it does guarantee convergence. The activity concentrations prior to and post partial volume correction are given in Table 1.

Table 1
Results of partial volume correction for measured phantom data: activity concentration (kBq/ml) before correction (BC) and after correction (AC) for the four syringes (true activity was 75 kBq/ml)

Syringe diameter (mm)	BC	AC	AC Sd
15	51.4	72.7	0.80
12	50.5	78.2	1.01
9	39.7	78.5	1.52
5	20.1	75.1	3.59

The recovery coefficient for the concentration in each syringe (percentage of the true signal) was low without partial volume correction ($\sim$70 % for the large syringe and $\sim$25% for the smallest). This shows how large partial volume effects can be, especially with small structures. When the presented algorithm was used, recovery was much better (90–110% recovery). Full results can be found in Aston et al. [12]. In addition, the method provides estimates of the associated error on these parameters which has not previously been possible.

3.2. Human data

[^{11}C]Flumazenil is a radiotracer which images the concentration of benzodiazepine receptors in the brain. A data set obtained from a human subject is shown in Fig. 4(a). The blurring kernel of the scanner was again approximately 6 mm in the x–y directions and 6.5 mm in the z-direction. The R matrix was determined from regional parcellation and tissue classification of a coregistered [8] structural MRI image. Whilst the coregistration is not perfect between the images, previous studies have shown this has little effect on partial volume correction when the misalignment is small [13]. The covariance structure of the noise in this image was completely specified by the D_1 matrix due to the prior temporal modelling. This allows for the application of the explicit solution given by Eq. (23). The regional concentrations, before and after partial volume correction, are given for a selected set of regions in Table 2.

For display, the local regional concentrations are projected back onto the anatomical parcellation (Fig. 4(b)). The concentrations shown in Fig. 4(b) and Table 2 have been shown to be well recovered using additional simulation studies and also compared to the results from other methods [12]. Without application of partial volume correction to the data it is evident that the concentrations can be significantly underestimated.

4. Discussion

A new algorithm has been presented for the application of linear models to multidimensional imaging data. It is based on the representation of a large matrix by
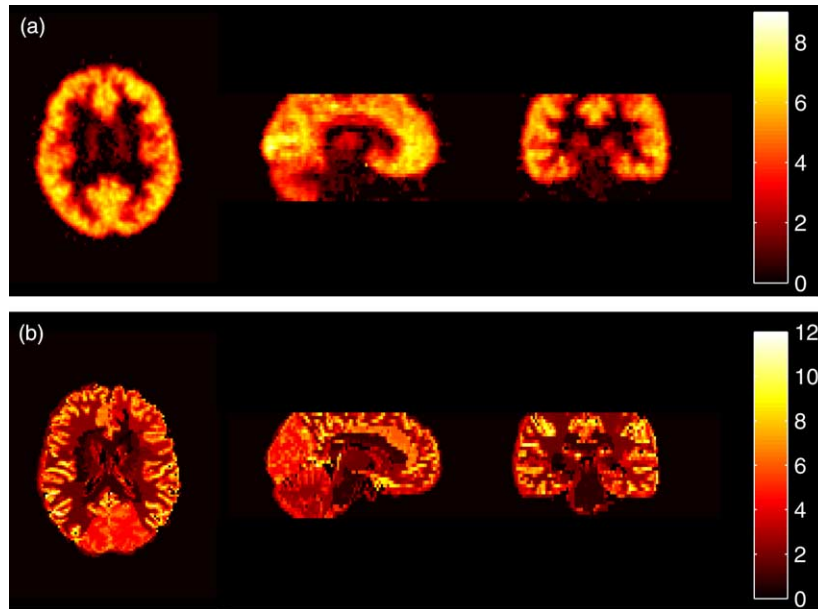
Fig. 4 Human [11C]Flumazenil images (volume of distribution) of benzodiazepine receptor concentration (ml of plasma/ml of tissue): (a) prior to partial volume correction, (b) projection onto anatomical parcellation after partial volume correction.

Table 2
Results of partial volume correction for measured human [11C]Flumazenil data: volume of distribution (ml of plasma/ml of tissue) values before correction (BC) and after correction (AC) for a representative set of anatomical regions (R—Right, L—Left)

Region	Grey matter			White matter		
	BC	AC	AC Sd	BC	AC	AC Sd
R Amygdala	3.30	7.21	0.39	2.78	0.48	0.38
L Amygdala	4.01	5.83	0.40	2.68	0.37	0.31
R Frontal Lobe	5.78	9.23	0.03	3.55	2.31	0.01
L Frontal Lobe	5.35	8.81	0.03	3.91	2.96	0.01
R Occipital Lobe	5.47	7.51	0.07	4.86	4.19	0.03
L Occipital Lobe	5.42	6.73	0.06	4.77	4.46	0.03
R Thalamus	2.10	4.76	0.20	1.55	1.81	0.04
L Thalamus	3.06	5.32	0.19	1.13	1.10	0.03
R Cerebellum	4.29	6.26	0.03	2.88	2.31	0.01
L Cerebellum	4.49	6.61	0.03	3.03	2.12	0.01

set of much smaller matrices which operate on the data through Kronecker products. Through the use of this multimatrix algorithm, it is now possible to use more complex linear models to address the problem of partial volume effects in PET. This

algorithm is general and has broader applications in neuroimaging and to other multidimensional data sets. For certain covariance structures an explicit solution is possible and for more complex covariance structures the solution is achieved through an iterative scheme. Conditions for convergence for the iterative method have been derived.

Several methods have previously been applied to the PET partial volume problem. These methods have been implicitly based on finding least squares solutions to the vectorisation of the problem (Section 2.1). However, these solutions were restricted to using simple forms for the covariance matrices which made the computation feasible. Labbé et al. [14] investigated the ordinary least squares solution to the problem which is equivalent to using $\Sigma = I$ in Eq. (2). Rousset et al. [15] took a different approach, that although not explicitly formulated as a least squares solution, is equivalent to taking $\Sigma = P^{T}$ in Eq. (2). However, in both methods, the inherent three-dimensional structure was not taken into account, and as such the process was incredibly time consuming even for a small volume and a small number of regions. The presented method offers a great improvement in computation time over previous methods (a factor of $50 \times$ faster—taking 30 min for one standard volume), and allows for more complex and accurate models to be applied.

This new algorithm is now in routine use in several large clinical imaging studies into neurological diseases such as epilepsy. Partial volume effects can have a major impact due to the structural changes in these pathologies. The tractability and rapid nature of these algorithms has permitted the analyses of functional brain imaging studies that were not previously possible.

Acknowledgements

References

[1] M.E. Phelps, Inaugural article: positron emission tomography provides molecular imaging of biological processes, Proc. Natl. Acad. Sci. USA 97 (16) (2000) 9226–9233.

[2] T. Jones, Present and future capabilities of molecular imaging techniques to understand brain function, J. Psychopharmacol. 13 (4) (1999) 324–329.

[3] T.G. Turkington, Introduction to pet instrumentation, J. Nucl. Med. Technol. 29 (1) (2001) 4–11.

[4] R.M. Leahy, J.Y. Qi, Statistical approaches in quantitative positron emission tomography, Statist. Comput. 10 (2) (2000) 147–165.

[5] R. Gunn, S. Gunn, V. Cunningham, Positron emission tomography compartmental models, J. Cereb. Blood Flow Metab. 21 (2001) 635–652.

[6] E.J. Hoffman, S.C. Huang, M.E. Phelps, Quantitation in positron emission computed tomography: 1. Effect of object size, J. Comput. Assist. Tomogr. 3 (3) (1979) 299–308.

[7] D.L. Collins, C.J. Holmes, T.M. Peters, A.C. Evans, Automatic 3D model-based neuroanatomical segmentation, Hum. Brain Mapp. 3 (3) (1995) 190–208.

[8] C. Studholme, D.L. Hill, D.J. Hawkes, Automated three-dimensional registration of magnetic resonance and positron emission tomography brain images by multiresolution optimization of voxel similarity measures, Med. Phys. 24 (1) (1997) 25–35.

[9] G.H. Golub, C.F. Van Loan, Matrix Computations, The Johns Hopkins University Press, Baltimore, USA, 1983.

[10] O. Axelsson, Iterative Solution Methods, Cambridge University Press, Cambridge New York, 1994.

[11] J. Kamm, J.G. Nagy, Kronecker product and svd approximations in image restoration, Linear Algebra Appl. 284 (1998) 177–192.

[12] J.A.D. Aston, V.J. Cunningham, M.-C. Asselin, A. Hammers, A.C. Evans, R.N. Gunn, Positron emission tomography partial volume correction: estimation and algorithms, J. Cereb. Blood Flow Metab. 22 (2002) 1019–1034.

[13] V. Frouin, C. Comtat, A. Reilhac, M.-C. Grégoire, Correction of partial-volume effect for pet striatal imaging: fast implementation and study of robustness, J. Nucl. Med. 43 (12) (2002) 1715–1726.

[14] C. Labbé, J.C. Froment, A. Kennedy, J. Ashburner, L. Cinotti, Positron emission tomography metabolic data corrected for cortical atrophy using magnetic resonance imaging, Alzheimer Dis. Assoc. Disord. 10 (3) (1996) 141–170.

[15] O.G. Rousset, Y. Ma, A.C. Evans, Correction for partial volume effects in PET: principle and validation, J. Nucl. Med. 39 (5) (1998) 904–911.